Fluid-Structure Interaction in Combustion System of a Gas Turbine—Effect of Liner Vibrations

A. K. Pozarlik
Laboratory of Thermal Engineering,
University of Twente,
P.O. Box 217,
Enschede 7500 AE, Netherlands
e-mail: a.k.pozarlik@utwente.nl

J. B. W. Kok
Laboratory of Thermal Engineering,
University of Twente,
P.O. Box 217,
Enschede 7500 AE, Netherlands

Prediction of mutual interaction between flow, combustion, acoustic, and vibration phenomena occurring in a combustion chamber is crucial for the reliable operation of any combustion device. In this paper, this is studied with application to the combustion chamber of a gas turbine. Very dangerous for the integrity of a gas turbine structure can be the coupling between unsteady heat release by the flame, acoustic wave propagation, and liner vibrations. This can lead to a closed-loop feedback system resulting in mechanical failure of the combustor liner due to fatigue and fatal damage to the turbine. Experimental and numerical investigations of the process are performed on a pressurized laboratory-scale combustor. To take into account interaction between reacting flow, acoustics, and vibrations of a liner, the computational fluid dynamics (CFD) and computational structural dynamics (CSD) calculations are combined into one calculation process using a partitioning technique. Computed pressure fluctuations inside the combustion chamber and associated liner vibrations are validated with experiments performed at the state-of-the-art pressurized combustion setup. Three liner structures with different thicknesses are studied. The numerical results agree well with the experimental data. The research shows that the combustion instabilities can be amplified by vibrating walls. The modeling approach discussed in this paper allows to decrease the risk of the gas turbine failure by prediction, for given operating conditions, of the hazardous frequency at which the thermoacoustic instabilities appear. [DOI: 10.1115/1.4026904]

Keywords: fluid-structure interaction, thermoacoustic instabilities, acoustics, vibrations

1 Introduction

The lifetime of a typical gas turbine engine is mostly limited by thermal and mechanical loads on the turbine blades and on the combustion chamber liner [1]. During lean premixed combustion, the turbulent flame with its enormous and fluctuating thermal power amplifies or damps acoustic pressure changes inside the combustion chamber [2,3]. The acoustic domain comprised of the combustion chamber, the burner internals, and the combustor air supply is acoustically closed, and only a minor part of the sound is able to leave it together with the exhaust gases [4]. The rate of dissipation of the acoustic wave energy in the combustion chamber is very low, and therefore, most of the sound is reflected from the walls and radiated into the flame, which is highly sensitive to acoustic perturbations. The sensitivity of the flame to acoustic wave excitation depends on several parameters, such as the equivalence ratio, flame length, and position. The acoustic source that the flame represents interacts with the propagated and the reflected pressure waves, and in case the Rayleigh's criterion [5] with later changes [6] is fulfilled, i.e., that the heat released by the flame and the pressure fluctuations are in phase, the oscillations can become unstable. Growth of the oscillations is possible if the energy gain exceeds the acoustic energy losses in the acoustic domain (see Eq. (1)). In that case, a self-exciting instability loop starts growing in amplitude until nonlinear processes impose a saturation limit. This process is known as a thermoacoustic instability.

$$\frac{(\gamma-1)}{\gamma p_0}\int_V\int_0^\tau p'Q'dtdV > \int_A\int_0^\tau p'\mathbf{u}dtdA \tag{1}$$

The origin of combustion instabilities is discussed in many publications, e.g., Refs. [4] and [7–9]. However, the fundamental mechanisms of the instabilities are difficult to recognize precisely. Oscillations in heat release or pressure fluctuations are produced by complicated mechanisms that influence each other; thus, the exact characterization of the source is in many cases impossible. Fluctuations in equivalence ratio, unsteady strain rate, swirl modulation, flame front kinematics, interactions between flame and vortex, or flame-boundaries interaction are a few of them [2,10–12]. Also, each of the above-mentioned processes depends on additional factors, like nozzle geometry, fuel kinetics, heating value, ambient temperature, and swirl conditions. These processes generate perturbations in rate of heat release by inducing oscillations in flame position or distortion of the enveloping area of the flame. The thermoacoustic instabilities may lead to a significant vibration amplitude of the liner and strong changes in the flame structure. Of crucial importance for the operation of the engine is not the noise emitted but its structural integrity, which may be hazardous when the combustor liner starts to vibrate in a mode linked to the thermoacoustic noise. The strong coupling between the acoustic fluctuations and liner resonance modes induces high-amplitude vibrations of the surrounding liner structure, feeding additional acoustic energy to the combustor volume and enhancing (or damping) the instabilities. The amount of energy transferred from the acoustic field inside the combustion chamber to the vibrating walls (and vice versa) is related not only to the amplitude of acoustic waves but also to the frequency and shape of the structural modes and damping in the system. The liner is a

Contributed by the Combustion and Fuels Committee of ASME for publication in the Journal of Engineering for Gas Turbines and Power. Manuscript received November 8, 2013; final manuscript received February 11, 2014; published online March 21, 2014. Assoc. Editor: Joseph Zelina.

critical component, because it has to operate reliably at extremely high temperatures. High-amplitude liner vibrations and reduced material strength due to high temperature, linked with long operational time, will lead finally to untimely fatigue damage of the liner [1,13].

Only a small number of investigations have focused on the fluid and structural interaction phenomena in a gas turbine combustor. The existing literature is mostly limited to modeling of one-way interaction, taking into account only the effect of the gas flow and/or acoustic pressure fluctuations on the liner and turbine blades structure (see Refs. [14–17]) but neglects the feedback mechanisms. The interacting phenomena, i.e., turbulence, heat transfer, acoustics, vibrations, gas flow, etc., have strong influence on each other; therefore, to predict the instabilities, a computational process must include a comprehensive interaction between fluid and structural field. This can be done efficiently by using two-way fluid-structure interaction approach (FSI). This paper presents a computational and experimental study of the mutual interaction between thermoacoustic instabilities and vibrations of the liner. Both flexible and rigid liner geometries are investigated. In the numerical simulations also a liner with uniform thickness is considered. For all the numerical studies, three numerical codes are coupled into one calculation process. The frequency and amplitude of thermoacoustic instabilities and liner vibrations are predicted and compared with experimental data.

2 Experiment

The investigated flame in a laboratory-scale elevated pressure combustor is a natural gas lean premixed flame. The experiments are performed in a laboratory test rig able to operate with maximum thermal power equal to 500 kW at 5 bar absolute pressure. The investigated combustion setup is intended to be representative for (a section of) an industrial-scale gas turbine (annular) combustion chamber. To obtain the acoustic eigenfrequencies of the test rig in the range of those presented in industrial designs, the length of the combustor is similar to commercial combustors (approx. 1.8 m). As a consequence, the flame is relatively small and occupies only the most upper part of the upstream section of the test rig. This solution is often applied to the experimental setups devoted for study of thermoacoustic instabilities [18,19]. Because of the slender construction, the circumferential acoustic modes are not present in the investigated frequency range [20]. To limit the temperature of the structural parts exposed to hot gases, a cooling flow between liner and pressure vessel is applied. Pressure transducers and thermocouples are located along the setup to collect temperature and pressure data at different positions. LABVIEW and SigLab hardware and software is used for data recording. The longitudinal cross section of the combustion test rig together with the location of data recording points is presented in Fig. 1 (left), where P and Ps are dynamic and static pressure sensors, respectively; T are thermocouples; LDV is a laser Doppler vibrometer; and CCD stands for the camera for chemiluminescence measurements. In a gas turbine, the liner should be stiff for a high first eigenfrequency and low amplitude of structural vibrations, but on the other hand, its thickness must be sufficiently small to assure low thermal stresses and avoid fatigue. This results in a liner design in a full-size engine, which has the lowest structural eigenfrequency usually around 200–500 Hz, depending on the design. To achieve that low first eigenfrequency in the current study with the small laboratory-scale structure, the liner was made with a section having reduced stiffness. The flexible section, located between stiff parts (see Fig. 1 (right)), ensures a low first eigenfrequency and a high sensitivity to the instantaneous pressure changes inside the combustion chamber. Any variations in the pressure pattern inside the combustion test rig are immediately related to changes in the vibration amplitude and frequency of the flexible section. To leave the liner vibrations undisturbed, all thermocouples and pressure transducers are located at some distance from the flexible section. Furthermore, to exclude effects of added

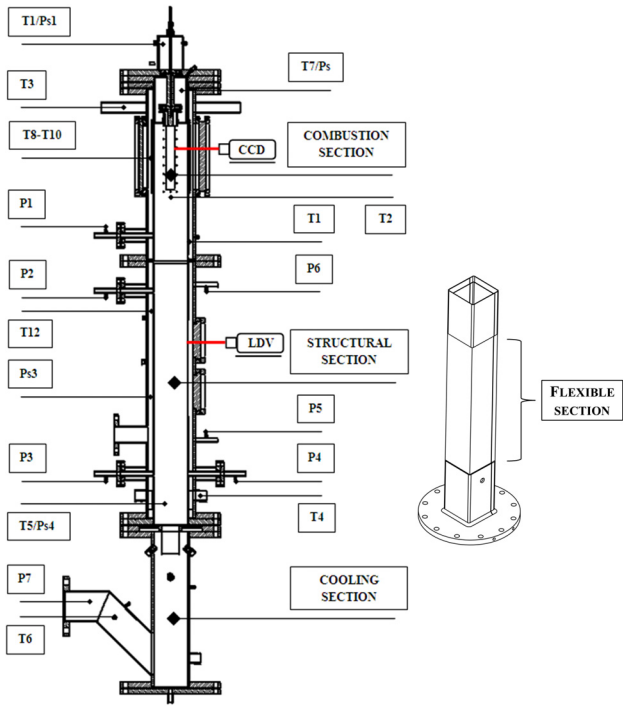

Fig. 1 Combustion setup configuration (left) with bottom part of the liner (right)

mass and stiffness to the flexible liner structure, a noninvasive laser technique, i.e., laser Doppler vibrometry, is used for vibrational data collection. Vibrations are measured through a slit window located at 25 mm from the corner of the liner, whereas the pressure signal is recorded with application of Kulite pressure sensors at the location of pressure transducer P2 (see Figs. 2 and 1, respectively). At the outlet of the combustion chamber, a contraction tube is located in order to provide a well-defined closed acoustical condition. The natural gas flow, combustion air flow, and cooling air flow are controlled by Bronkhorst mass flow controller. Natural gas is provided from the grid, boosted to 10-bar pressure by a screw compressor driven by a 15-kW electric motor, whereas the air is dried and then pressurized to 10 bar by a screw compressor driven by a 160-kW diesel engine. The combustion air could be preheated to 300 °C by a 80-kW electric heater. The

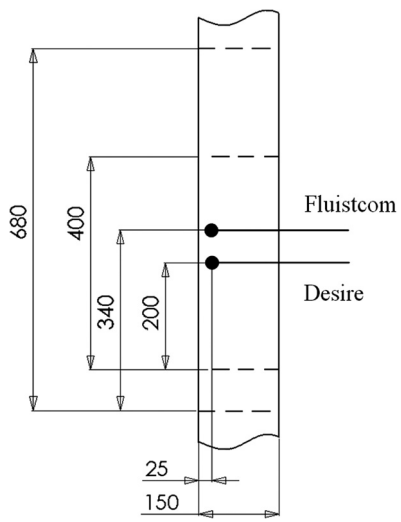

Fig. 2 Location of the vibration measurements inside the flexible section

Table 1 Operating conditions and liner dimensions

Combustible flow				
Power	Abs. pressure	Air factor	Mass flow rate	Air temperature
125 kW	1.5 bar	1.8	75.53 g/s	573 K

Dimensions and material properties of the liner (high temperature)					
	Length rigid/flexible part	Thickness rigid/flexible part	Width	Young's modulus	Poisson's ratio
Desire	1813/400 mm	4/1.5 mm	150 mm	138 GPa	0.3
Fluistcom	1813/680 mm	4/1.0 mm			
Uniform	1813/1813 mm	2/2.0 mm			

dynamics of the flame, acoustics, and liner and their response to excitation was determined by variation of the transient gas flow by means of a MOOG valve.

Two liner configurations with different thicknesses and lengths of the flexible section are investigated (see Table 1). The liner called Desire represents the almost rigid wall configuration, whereas the Fluistcom liner is much more flexible. Both names, i.e., Desire and Fluistcom, come from the names of the European projects during which the liners were manufactured. The third construction investigated in this paper, i.e., liner with uniform thickness, was not investigated experimentally.

The lean premixed natural gas flame is investigated under conditions presented in Table 1. For the reference, the equivalence ratio controlled by the MOOG valve is oscillated with frequency of 300 Hz and amplitude equal to 8.5% of the mean equivalence ratio. During the experiment, the pressure and velocity signals are recorded with the use of SigLab hardware and software in a frequency range up to 2 kHz. A total number of 8192 samples per bandwidth is taken, which gives the frequency resolution equal to 0.24 Hz. In order to eliminate randomness in the recorded signal, data in the frequency domain are averaged over 20–40 measurements. Due to restrictions imposed by the SigLab hardware, in the time domain, only the last measurement is saved [21].

3 Numerical Models

The investigated reacting flow is resolved by using the finite volume method (ANSYS-CFX 11 [22]), whereas the structural vibrations are calculated by application of the finite element method (ANSYS-MULTIPHYSICS 11 [23]). For convenience, later in the paper, ANSYS-MULTIPHYSICS 11 is referred as ANSYS and ANSYS-CFX 11 as CFX. Data exchange between codes is performed with application of the MFX coupling code.

The acoustic phenomenon in the gas turbine combustors originate from different sources. Vibrating walls, regions of turbulent flow, and mixing of fluids with different temperatures are only a few examples of sound-generation mechanisms. Sir James Lighthill has identified and classified these mechanisms as the monopole, dipole, and quadrupole source [24,25]. A flame in the combustion chamber behaves like a monopole acoustic source. The external nonuniform force exerted on the gas inside the combustion chamber originates mainly from the vibrating walls and acts as dipole. The turbulence field inside the combustion is generated by the second order gradient of the velocity and therefore is a quadrupole source.

The analysis performed on the different types of sources in the combustion chamber [26] shows that the acoustic power from the combustion process (monopole sound) is the strongest. It is bigger by about $1/\mathrm{Ma}^4$ than the acoustic power generated by the unsteady turbulence field (quadrupole source). Since the combustor operates on a low Mach number ($\mathrm{Ma} \cong 0.1$) [27], the quadrupole source can be neglected. The effect of the dipole source on the acoustic field in the combustion chamber strongly depends on the stiffness of the walls.

3.1 CFD Model. The governing equations describing a time-dependent viscous combustible and compressible flow are in Cartesian coordinates in the following:

$$\text{Continuity:}\quad \frac{\partial \rho}{\partial t} + \frac{\partial \rho u_i}{\partial x_i} = 0 \tag{2}$$

$$\text{Momentum:}\quad \frac{\partial \rho u_j}{\partial t} + \frac{\partial}{\partial x_i}\left(\rho u_i u_j\right) = -\frac{\partial p}{\partial x_j} + \frac{\partial \tau_{ij}}{\partial x_i} \tag{3}$$

$$\text{Species:}\quad \frac{\partial \rho Y_k}{\partial t} + \frac{\partial}{\partial x_i}\left(\rho u_i Y_k\right) = -\frac{\partial}{\partial x_i}\left(V_{k,i} Y_k\right) + \dot{\omega}_k \tag{4}$$

$$\text{Enthalpy:}\quad \frac{\partial \rho h_s}{\partial t} + \frac{\partial}{\partial x_i}\left(\rho u_i h_s\right) = \frac{Dp}{Dt} - \frac{\partial q_i}{\partial x_i} + \tau_{ij}\frac{\partial u_i}{\partial x_j} + \dot{\omega}_T \tag{5}$$

The viscous stress tensor and the energy heat flux are indicated with τ_{ij} and q_i, respectively. They can be modeled with the classic Newtonian fluid constitutive equation and the Fourier heat transfer law, as shown in Eq. (6) for τ_{ij} and Eq. (7) for q_i.

$$\tau_{ij} = -\frac{2}{3}\mu\frac{\partial u_k}{\partial x_k}\delta_{ij} + \mu\left(\frac{\partial u_i}{\partial x_j} + \frac{\partial u_j}{\partial x_i}\right) = -\left(P_{ij} - p\delta_{ij}\right) \tag{6}$$

$$q_i = -\lambda\frac{\partial T}{\partial x_i} + \rho\sum_{k=1}^{N} V_{k,i} Y_k h_{s,k} \tag{7}$$

where δ_{ij} is the Kronecker symbol equal to 1 when $i = j$; otherwise, $\delta_{ij} = 0$. Y_K is the mass fraction, $V_{k,i}$ are the diffusion velocities, $\dot{\omega}_k$ is reaction rate of species k, and $\dot{\omega}_T$ is heat release due to combustion described as $\dot{\omega}_T = -\sum_{k=1}^{N} \Delta h^0_{f,k}\dot{\omega}_k$ Enthalpy h_s is the sensible enthalpy written in the form given by Ref. [28].

3.1.1 Turbulence Model. Instead of representing the turbulence exactly in time and spatial scale, models for the statistical approximation of the turbulence effect on the mean or averaged flow properties are often used. In this work, the scale adaptive simulation (SAS) [29] is applied. The main advantage of this model is its high ability to capture unsteady flow features, more precisely than standard unsteady Reynolds-averaged Navier–Stokes (URANS) due to the von Karman length scale introduced into the exact transport equation for the integral length scale [30–32]. Since the SAS model is combined only with the shear stress transport (SST) turbulence model, further in the paper is referred as SAS.

3.1.2 Combustion Model. For reacting flow calculations, a single-step combustion model is used. The model determines the rate at which a component is consumed or created in a single reaction step during the combustion process. The eddy dissipation/finite rate chemistry (ED/FRC) model is applied to calculate reactions occurring in the flame. Combining the ED and FRC approach allows us to capture the whole range of Damköhler numbers in the reacting flow. The effective reaction rate is the minimum of the FRC and the ED rate [22]. This is applied for each reaction step separately; thus, while the rate for one step may

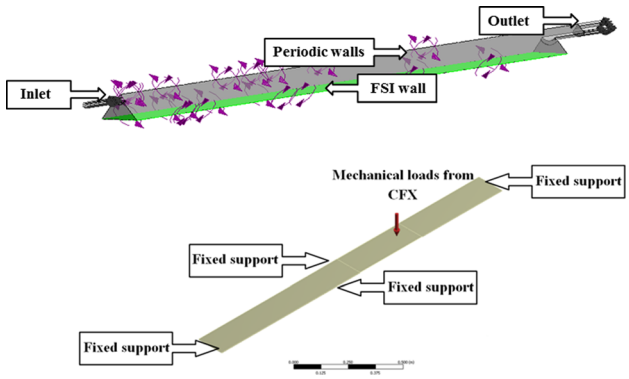

Fig. 3 Geometry and boundary conditions for CFD (top) and CSD (bottom) analysis

be limited by the chemical kinetics, some other step might be limited by the turbulent mixing at the same time and physical location.

3.1.3 CFD Computational Domain and Setup. The investigated combustor is fired by a premixed natural gas flame under conditions presented in Table 1. To save computational time and to reduce the number of mesh elements, the numerical domain is restricted to a quarter section of the real combustion chamber, with periodic boundary conditions (see Fig. 3 (top)). A total number of 720,000 unstructured elements is used for the calculations. The appropriate mesh size is chosen on basis of a previously performed mesh independency study. To capture the flame properties, the flows in the inner and outer recirculation zones that are stabilizing the flame must be predicted accurately. Therefore, the majority of the elements are located in the flame and recirculation regions. The near-wall region is created with the use of prism elements to avoid generating highly distorted tetrahedral elements. The velocity and turbulence profiles at the inlet of the combustion chamber are imported from the separately made steady-state calculations (including the entire geometry with pressure decouplers, plenum, and swirler). A heat transfer coefficient is imposed on the vibrating wall. Other walls have adiabatic no-slip boundary conditions. In line with the experimental conditions, transient computations are performed with forced oscillations of the fuel-to-air equivalence ratio (frequency of 300 Hz and amplitude of 8.5%). A static average pressure is imposed at the outlet of the chamber to mimic the reflective acoustic boundary conditions of the experiment.

Resolving accurately the compressible unsteady Reynolds-averaged Navier–Stokes equations for acoustic waves propagation in turbulent combustible flow, a high grid resolution and small time step are necessary. The relation between the mesh resolution and time step for acoustics is given by the Courant–Friedrichs–Lewy (CFL) number, where $\mathrm{CFL} = (u + c)\,\Delta t/\Delta x$. Here, Δt is the time step and Δx stands for the length interval. The CFL number should be less than unity to ensure computational stability and accuracy when solving the URANS equations numerically. This makes prediction of the acoustic field, including flow, combustion, and vibrations, a very time-consuming and costly process. Calculations with the CFL number above unity are possible for the implicit numerical schemes, but numerical dissipation and dispersion increase together with the CFL number. Dissipation damps the acoustic pressure amplitude, and dispersion influences the propagation velocity in a frequency-dependent way [33]. The longer the propagation distance and the higher the frequencies involved in the process, the more significant the errors become. Introduction of higher than second-order methods in the CFD analysis can decrease errors made by numerical damping [34] but also extends computational time.

To reduce the computational effort, calculations with the CFL number higher than unity are performed (volume average CFL = 11). The second-order backward Euler transient scheme is used for calculations. The CFX code is an implicit scheme that is stable even during transient calculations with the CFL number above unity. Since investigated instabilities are not located in the high-frequency range, it is expected that numerical dissipation and dispersion have a minor influence on the results. Due to computational expenses, only about 100 ms of real time process is investigated.

3.2 FEM Model for Structural Motion. The model equations for the dynamics of the combustion chamber wall are solved by means of the implicit FEM code ANSYS 11. The liner of the combustion test rig is constructed of two parts connected by a sliding connection. This design will prevent accretion of thermal stresses due to expansion caused by heating up the structure to operational temperatures of about 800 °C, as both liner parts can freely expand in axial direction. Therefore, in the computations, the influence of thermal stresses can be neglected. Similar to the combustible flow model, the computational domain of the structural model is reduced and only one wall is investigated. The connections for pressure transducers and thermocouples, as well as the sliding connection between both liner sections, are located on the rigid part of the liner, and their influence on the vibration amplitude is minor. Thus, the geometry is simplified to a solid wall with a flexible section located between rigid plates. The side parts of the liner are clamped. Mechanical loads, i.e., pressure and shear from the CFX calculations, are transferred and applied as boundary conditions to the inner liner surface (see Fig. 3 (bottom)). A total number of 19,000 equally distributed 10-nodes SOLID92 tetrahedral elements with quadratic displacement behavior [23] are used for dynamic calculation. The material properties of stainless steel 310 adequate to uniform liner temperature of 760 °C are applied (see Table 1). The structural and fluid fields are solved synchronized for each time step. In the current setup configuration, it is impossible to measure pressure changes at the same location as the liner vibrations; therefore, the numerical data are compared with the experimental measurements at two positions: for pressure data at location of the pressure transducer P2 (the closest pressure sensor to vibrating walls) and for the liner vibrations in the middle of the flexible section (see Figs. 1 and 2).

In the above-described liner model, it is possible to study the effect of wall flexibility on the thermoacoustic instabilities; however, it is difficult to assess the importance of the location of vibrations. Therefore, an additional numerical model of the liner, with uniform thickness of 2 mm and first structural eigenfrequency between those of Desire and Fluistcom, is investigated. Other model conditions are unchanged.

4 Numerical Procedure

To investigate interacting phenomena in the combustion system, the partitioned approach is used. In this approach, fluid and structural models are considered as isolated entities and the boundary solutions of one process are used as the boundary conditions for the other process. Separate codes work independently using different numerical techniques to solve fluid and structural subdomains along the fluid-structure interface [35–39]. Exchange information via coupling code is performed every iteration or time step up to the moment convergence is obtained.

For the strongly dependent on each other mechanisms, where changes in one of the coupled fields directly influence the other field and vice versa, a two-way coupling is necessary. In the two-way interaction process, the CFD and CSD codes are forced to dynamically exchange information every time step. Due to control volume change of the elements over time during calculations with the moving mesh (in CFD), the governing equations must be modified. Therefore, the term W_j representing the velocity of the control volume boundary was introduced [22]. After modification, the resulting equations are in the form of Eqs. (8) and (9). Regions

of nodes with the same degrees of freedom are determined by the mesh stiffness according to Eq. (10),

$$\frac{d}{dt}\int_{V(t)} \rho dV + \int_S \rho(u_j - W_j)dn_j = 0 \tag{8}$$

$$\frac{d}{dt}\int_{V(t)} \rho u_i dV + \int_S \rho u_i(u_j - W_j)dn_j = -\int_S P dn_j + \int_S \mu_{\text{eff}}\left(\frac{\partial u_i}{\partial x_j} + \frac{\partial u_j}{\partial x_i}\right)dn_j + \int_V S_{u_i} dV \tag{9}$$

$$\nabla \cdot \left(\Gamma_{\text{disp}} \nabla \delta\right) = 0 \tag{10}$$

In Eqs. (8)–(10), V is the cell volume; S is the surface; dn_j are the differential Cartesian components of the outward normal surface vector; μ_{eff} is the effective viscosity defined as $\mu_{\text{eff}} = \mu + \mu_t$, where μ is the dynamic viscosity and μ_t the turbulent viscosity; Γ_{disp} is the mesh stiffness; and δ is the displacement related to the previous mesh position.

A uniform mesh stiffness is used. Displacement is homogenously spread through the mesh. The remaining internal nodes have their position adjusted while the mesh topology is preserved. Thus, the regions with higher elements density after upgrading the mesh, according to the data from the FEM analysis, stay finer than the rest of the grid. Equations (9) and (10) are solved at the start of each iteration or time step for the CFD computations [22].

To increase stability of calculations, a serial coupling was chosen. In the serial coupling, the fluid and structural solvers work alternately. All fields are solved in successive steps, and the coupling is done at the end of the iteration or time step. During the call, all necessary loads are collected from one field and sent to the other solver. The stagger loop is done once per time step, making the process a weak coupling. The weak coupling is a very efficient technique and is applicable for coupled fields having significant difference in density or in the characteristic time scale [40,41]. In the current study, the ratio between density of hot gases and hot structure is of the order of $\rho_f/\rho_s = \mathcal{O} \sim 10^{-5}$. The computational time step of the turbulent combustible flow, including propagation of the acoustic wave, depends on the mesh resolution. However, in most cases, the time step used for turbulent flow calculations is of the order of $\mathcal{O} \sim 10^{-5}$ s, whereas for the structural analysis, the time step in the order of $\mathcal{O} \sim 10^{-2}$ s is sufficient. Furthermore, from the experiments, it is known that vibration amplitudes are small ($\mathcal{O} \sim 10^{-4}$ m). These observations promote the weak coupling method presented in Fig. 4.

To assure lossless data transfer through the fluid-structure interface, both fluid and structural models must have the same dimensions and global coordinates. The meshes on both sides of the interface connection are not matching; therefore, the globally conservative interpolation and the profile preserving interpolation [23] are used.

5 Modal Analysis

In order to assess the origin of some of the signals visible in the computed frequency spectra of pressure oscillations, a modal analysis of the investigated (fluid and structural) domains is performed. The modal analysis itself can indicate the eigenfrequencies of the instabilities, but it is not able to predict whether, for given operation conditions, the instabilities actually will appear. The flame properties depend on the fuel used for combustion, which can be affected by addition of hydrogen or by different methane content (e.g., natural gas from different parts of the world). This, in consequence, has influence on the appearance of the thermoacoustic instabilities, but it is not visible in the modal analysis.

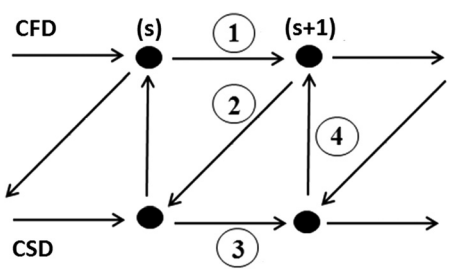

Fig. 4 Weak coupling algorithm

Acoustic, structural, and coupled modes were studied under steady-state conditions occurring during the combustion process in the combustion chamber (i.e., enhanced temperature, increased speed of sound, decreased Young's modulus, etc.). The structural modes are investigated in a simplified computational domain with clamped bottom and top edge conditions, whereas for the acoustic modes, the fluid domain is enclosed by acoustically hard walls. Coupled fluid-structural modes are evaluated for a fluid domain surrounded by flexible structural walls. In the latter analysis, frequencies at which the structural and acoustic modes exist together are called isochronism points. The isochronism points are hazardous for combustion systems, because the acoustic and structural eigenfrequencies can be excited simultaneously, leading finally to unstable combustion and to liner failure. Because the acoustic modes are investigated at the same operating point, it is assumed that the average speed of sound is constant for all three cases. The structural and coupled modes are unique for each of the liner configurations. The frequencies of the isochronism points are similar for all geometries; however, different structural modes are observed in the vicinity of the isochronism point. Thus, the effect of the coupled modes on the system behavior can be different. Full modal and acoustoelastic analysis of the investigated systems can be found in Ref. [20].

6 Results

While coupling calculations in two numerical domains into one computation process, the partitioning error, which may appear during data exchange through the interface, can have a significant influence on the obtained results. Therefore, the partitioning error created on the interface connection during the interpolation process is investigated. Taking into account that the mesh distortion process in the CFD requires more computational effort than the force transfer, the displacement on both sides of the interface connection is compared. It is concluded that the coupling algorithm works well (see Fig. 5). Displacements on the structural and fluid face are similar. Only a minor error without significant impact on the calculations is observed.

6.1 Modal Analysis. The combustion chamber of the setup is characterized by a high length/width ratio; therefore, acoustic modes visible in the investigated frequency range are limited to a longitudinal shape. Four acoustic modes are found. They are presented together with the associated eigenfrequencies in Fig. 6. It has been discussed in Ref. [20] that acoustic modes having local air compression or rarefaction are the most hazardous. Since the number of structural modes in the frequency range up to 1 kHz is significant and the mode shape and frequency is unique to the investigated liner geometry, only the first 50–70 structural modes per case are investigated. Instead, the coupled modes, especially in the frequency range near the hazardous acoustic modes, are evaluated. The most energetic modes giving the strongest feedback to the system are again the coupled modes, which show major air compression or rarefaction. These volumetric synchronized modes have strong influence on the instabilities due to the significant change of volume.

For the stiff liner (Desire) configurations, the synchronized modes appear at frequencies of 429 Hz, 446 Hz, 657 Hz, and 670 Hz. The two former modes present a pattern of the second acoustic mode and are coupled with the third symmetrical

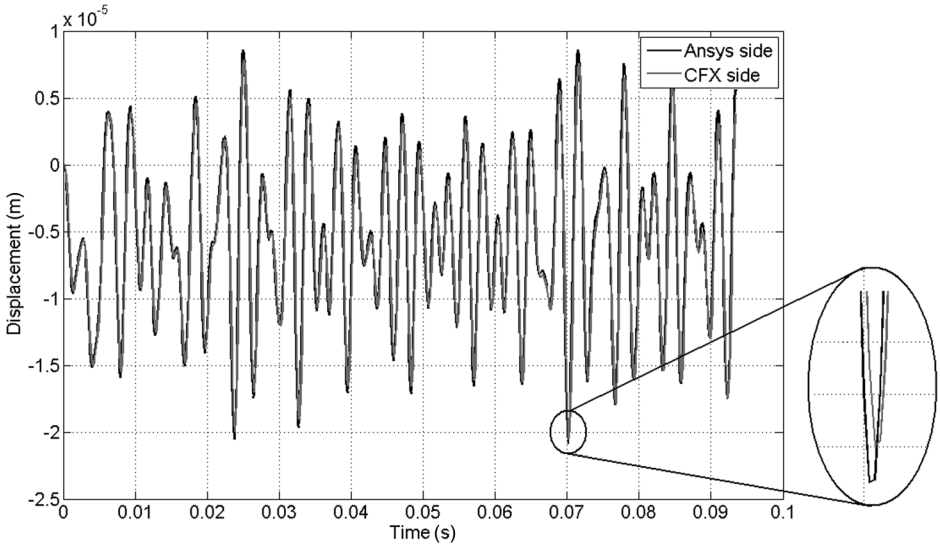

Fig. 5 Displacements comparison on the fluid and structure side

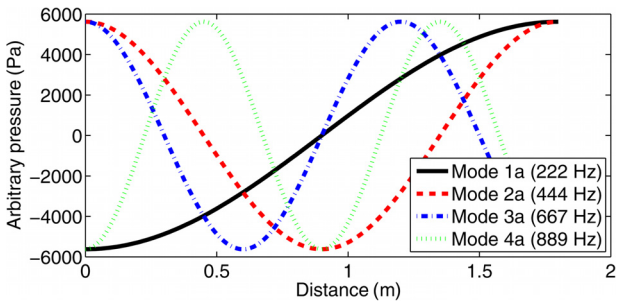

Fig. 6 Acoustic modes and eigenfrequencies of the combustion chamber

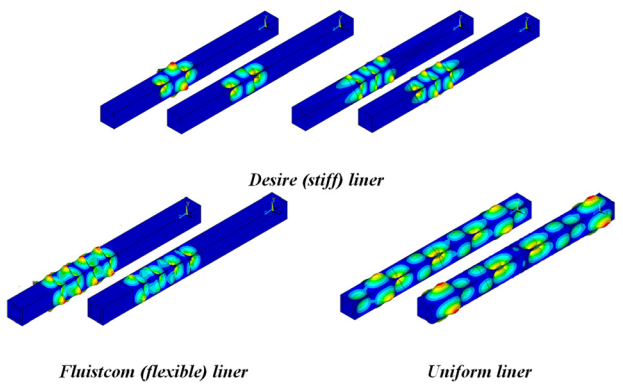

Fig. 7 Structural modes coupled with second acoustic mode

structural mode, whereas the other two are shaped as the third acoustic mode and coupled with the fifth structural mode (see Fig. 7). It is expected that the above-mentioned modes can lead to high-amplitude oscillation when they are excited. At the frequency of 219 Hz, another isochronism point exists. The structural mode at that frequency is also coupled with an acoustic mode. However, the pressure distribution during this mode is uniform, with maxima at both ends of the chamber, giving only a minor excitation by means of feedback to the system. The other, potentially hazardous modes are at a frequency of 312 Hz, 354 Hz, and 542 Hz. Those modes are dominated by the structure, but they cause a similar pressure distribution inside the combustion chamber as the acoustic modes. Because of the lack of acoustic modes with similar eigenfrequencies, these modes do not have a significant influence on the thermoacoustic instabilities.

At the frequency of 428 Hz and 445 Hz, the most energetic modes for the flexible liner (Fluistcom) configuration are observed. The second acoustic mode is coupled with the eighth (unsymmetrical) structural mode (see Fig. 7). However, the shape change of the structural modes did not influence the thermoacoustic instabilities (comparing to Desire liner), suggesting that the instabilities are closely related to the location and shape of the acoustic modes, and the influence of the structural modes in the above-mentioned cases is minor. Other possible hazardous coupled modes have their origin in structural vibrations, and hence, their effect on the thermoacoustic instabilities is negligible. At 223 Hz, an isochronism point exists (first acoustic mode coupled with structural mode), but similar to the Desire configuration, the contribution of this mode to pressure instabilities is minor.

Mapping the modal results onto the experimental pressure spectrum presented in Figs. 8 and 9, it can be found that the volumetric synchronized modes cover the regions where instabilities occur.

Since the thickness of the flexible section of the Desire and Fluistcom geometry is significantly smaller than the entire liner thickness, the structural modes appear mostly there. Thus, it is difficult to assess the mode shape and frequency effect on the flame located far from the vibrating section. This is studied with application of the uniform liner. In the uniform liner configuration, there are 13 potentially hazardous modes in the frequency range up to 500 Hz. Most of them have their origin in structural vibrations and they are not harmful to the system. The exceptions are modes at 454 Hz and 464 Hz, where the second acoustics eigenfrequency is coupled with the ninth symmetrical structural mode, as shown in Fig. 7. These modes are in the vicinity of the flame, and therefore, they have direct influence on the acoustic source and thermoacoustic instabilities. At the frequency of 215 Hz, another isochronism point exists (with first acoustic mode), but its effect on the instabilities is minor (similar to the stiff and flexible liner configuration).

6.2 Desire Liner. In order to compare the results of the FSI calculations with the conventionally used CFD models that neglect the effect of vibrating walls, additional CFD computations of the process were performed. Both the CFD and FSI analysis of the Desire (rigid) liner configuration have predicted the amplitude of pressure fluctuations, which is about 43% lower than observed during the experiment (based on root-mean-square (rms) value) (see Fig. 8). Due to high computational costs, only about 100 ms

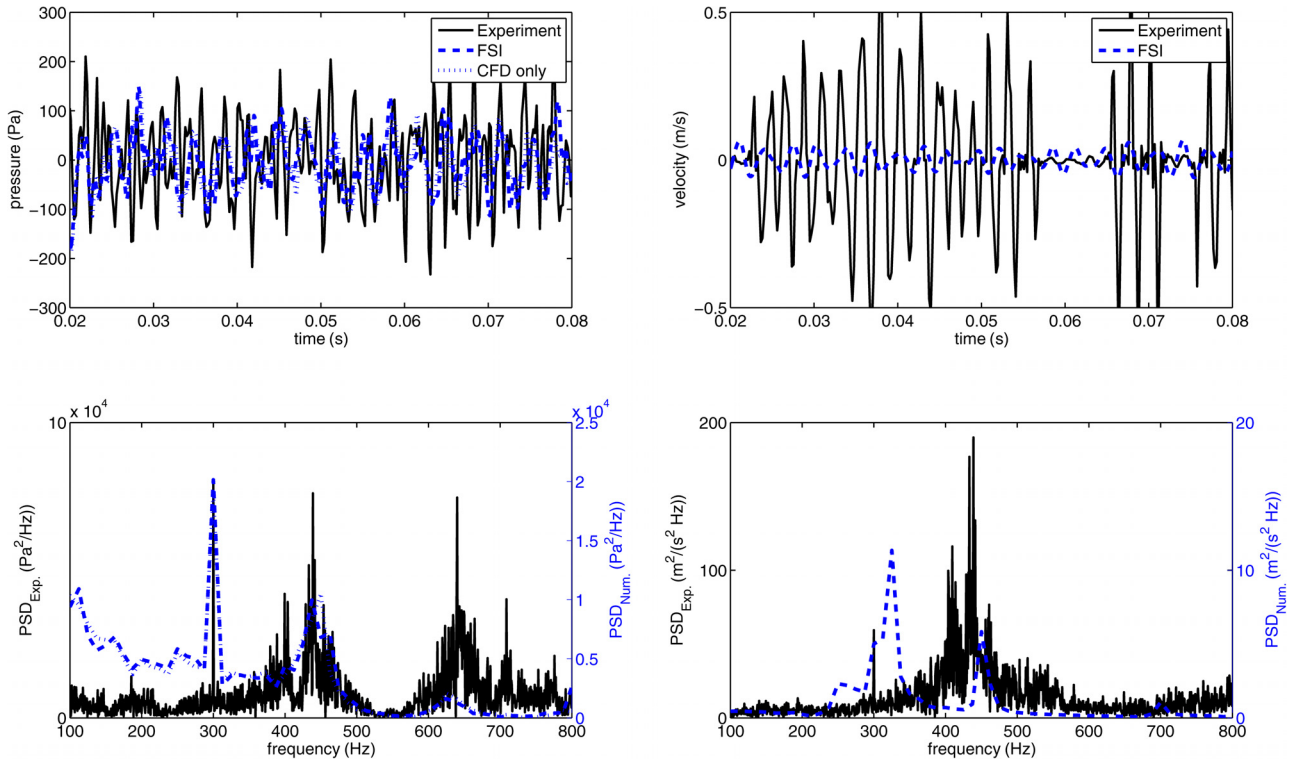

Fig. 8 Comparison of the numerical results with experimental data for the rigid (Desire) liner configuration

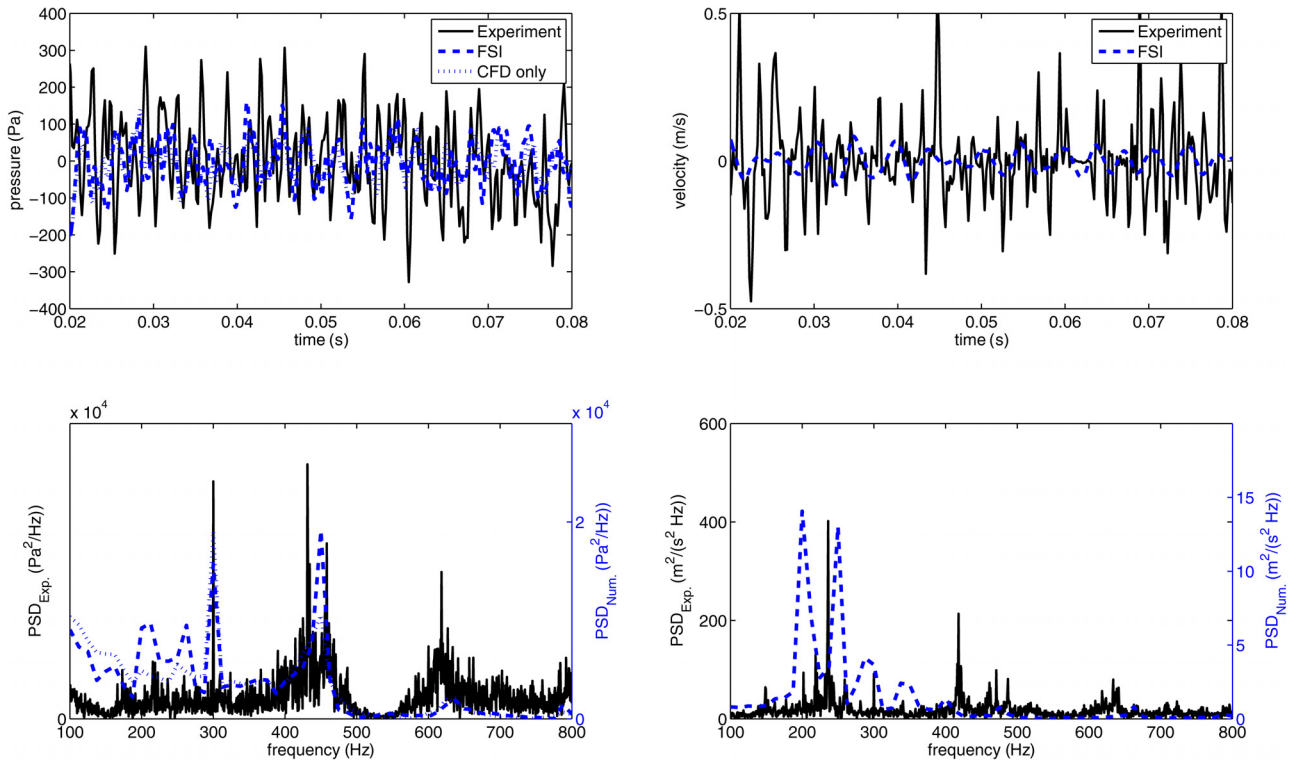

Fig. 9 Comparison of the experimental and numerical results of the pressure and velocity signal in time and frequency domain for the flexible liner configuration

of the combustion process is investigated during the numerical computations. Within such short time, the amplitude of the acoustic instabilities does not grow up to the saturation level. However, extension of the calculated process to a few seconds, necessary for instabilities to reach the correct amplitude, would result in enormous computational time. Numerical damping of the acoustic wave (CFL > 1) and simplifications of the fluid and structural domains also influence the results. The most visible thermoacoustics instabilities observed during the experiment are located at 439 Hz and 640 Hz. The observed 300 Hz signal is the forcing

pulsation frequency. The slightly bigger peak at 439 Hz is the main frequency of instabilities. The two-way FSI model shows the forcing peak at 300 Hz and the main instabilities at 438 Hz. This is exactly matching with the experimental data. An additional peak, predicted by the computations at 463 Hz can be recognized in the experimental spectrum as well. The instability at 625 Hz is also in the vicinity of experimental results (640 Hz). The 15-Hz discrepancy in frequency can be explained by the differences in the temperature field obtained during the numerical calculations with respect to the experiment and more significant numerical dispersion at high frequencies. Nevertheless, the prediction of the main instability frequency almost without error and the secondary instability with 2.5% error is a very satisfactory result. The model neglecting the vibrating wall effects also predicted well the main instabilities: the primary peak at 450 Hz and secondary at 625 Hz. However, most of the minor instability peaks visible in the experimental spectrum are not present in the CFD analysis.

The computed velocity amplitude is underpredicted by 52%, based on rms value from computational and experimental time of about 0.1 s and 3.2 s, respectively. This is a consequence of underprediction of the pressure amplitude by the CFD code, which is the main driving force for the wall vibration. Additionally, the cooling passage, which is not included in the numerical model, and the assumed uniform temperature along the liner have effect on the prediction of the vibrating wall behavior. The experimental data of the liner vibrations induced by the acoustic field have shown the forcing peak at 300 Hz and a main instability at 439 Hz (see Fig. 8). This matches well with the frequency of pressure instabilities inside the combustion chamber. The two-way numerical simulation has predicted the instabilities at 450 Hz, which gives a 2.5% error with comparison to the experimental data. Unexpectedly, the strongest vibrational peak is predicted at the frequency of 325 Hz. This peak is hardly visible in the experimental results. A separately made modal analysis shows in the vicinity of this frequency a strong first structural mode (312 Hz). Knowing that the velocity signal is recorded in the middle of the flexible section, it is most likely that the observed peak at 325 Hz comes from it. Since the pressure and velocity signal are evaluated at different locations, this peak is not visible in the pressure spectrum. This suggests only local influence of the vibrating wall on the pressure spectrum.

The results for the prediction of two-way interaction for the Desire liner configuration are in good agreement with the experimental data. It can be noticed that the effect of the vibrating walls is minor and does not have major impact on the overall instabilities in the system.

6.3 Fluistcom Liner. Similar differences between numerical results and experimental data, as during examination of the rigid configuration, are observed for the flexible liner geometry. Numerical results based on the rms value of oscillations show approx. 40% underprediction of the pressure amplitude inside the combustion chamber as compared to the experimental data.

In the experimental frequency spectrum, next to the forcing peak at 300 Hz, the primary thermoacoustic instabilities at 431 Hz and 458 Hz and secondary at 618 Hz are visible (see Fig. 9). Peaks at similar frequencies are observed in the numerical spectrum. The computations have predicted the primary instability at 450 Hz, which gives 4% or 2% error, depending on frequency of instabilities (i.e., 431 Hz or 458 Hz) promoted with time during the experiment. The valley free of instabilities between 500 Hz and 600 Hz is well visible in the FSI model as well. The secondary instability peak is located at 638 Hz. This gives 4% discrepancy from experimental results. The error between experiment and numerical data grows with increasing frequency. In the frequency range below 1 kHz, it has a maximum of 6%. The instabilities predicted by the numerical model between 200 and 263 Hz are in the vicinity of the first acoustic mode of the combustion chamber (220 Hz). They appear due to coupling of this acoustic mode with nearby located structural modes (first to fourth) of the relatively flexible liner. This behavior is also visible in the experimental spectrum of the liner vibrations.

The CFD computations of the combustion process only, not taking into account wall vibration, show also, in the Fluistcom case, very similar results of pressure fluctuations to the calculations, taking into account FSI. The major difference between results obtained from the models is in the ratio of the amplitude at the thermoacoustical instability to the reference peak at the forced frequency of 300 Hz. The dominant frequency spectrum peak in both the experimental and the FSI computational results is located at the frequency of thermoacoustic instabilities, i.e., it is noticeably bigger than the reference peak at 300 Hz. The CFD computations performed in the conventional way, without FSI, have shown the frequency of 300 Hz as dominant. For the assessment of the role of instabilities in system failure, a correct prediction of the most significant peaks is crucial, and hence, it can be concluded that it is important to take into account FSI.

In experiments, the dominant frequency of vibrations is observed at 236 Hz, followed by 418 Hz and the forcing frequency at 300 Hz. The numerical computations show main peaks at 200 Hz, 213 Hz, and 250 Hz; this is in the neighborhood of the main vibration frequencies observed in the experiment. However, the vibration frequency of 418 Hz is hardly visible. Further experimental studies have shown a competition between liner vibrations at frequencies of 236 Hz and 418 Hz. This can be an effect of variation in the main frequency of thermoacoustic instabilities, instantaneous changes in the liner temperature, or coupling between pressure oscillations and wall vibrations near the first acoustic mode.

For the Fluistcom liner (similarly to the Desire liner), vibrations of the flexible section located far from the flame are not able to give significantly high energy input to affect considerably the acoustic pattern inside the combustor.

6.4 Uniform Liner. In addition to the relatively rigid (Desire) and flexible (Fluistcom) walls configuration, which share the fact they have a 4-mm liner thickness for most of the length, with the exception of a short test section with reduced thickness, a liner with overall uniform thickness of 2 mm was investigated numerically. For this liner model, it was found that the amplitude of the pressure fluctuations (Fig. 10) is rapidly growing up to its saturation level. Within 0.1 s, the instabilities are already at a level of 2 kPa, which is about ten times bigger in comparison to the pressure fluctuations observed in the model without vibrating walls. The high-amplitude pressure fluctuations lead to a strong instability peak at frequency of 462 Hz. The reference peak with forced excitation at 300 Hz is almost invisible. The rapid growth rate of the thermoacoustic instabilities has its origin in the acoustic source induced by the vibration of the liner in the close proximity of the flame (as presented in Fig. 7). In case of the other two liner configurations, the walls have the flexible section far from the flame; thus, the energy input to the acoustic field upstream of the flexible section, i.e., in the flame vicinity, is minor. In consequence, there are only minor changes in the amplitude and frequency of pulsation. It has to be noted that the vibrating wall also influenced the frequency of the instabilities, moving it to 462 Hz. This slight shift can be caused by the structural mode coupling with the second acoustic eigenfrequency.

The vibration amplitude of the liner with uniform thickness is also enhanced in comparison to the behavior predicted in the other situations. However, the excited modes are in the proximity of the first acoustic frequency, i.e., at 200 Hz and 250 Hz. These modes come from coupling between the first acoustic eigenfrequency with neighboring structural frequencies.

The uniform configuration most resembles the industrial liner (i.e., no flexible part clamped between two stiff liner sections, no sliding connection, etc.). The feedback from the vibrating walls to the flame is sufficiently strong to enhance the combustion

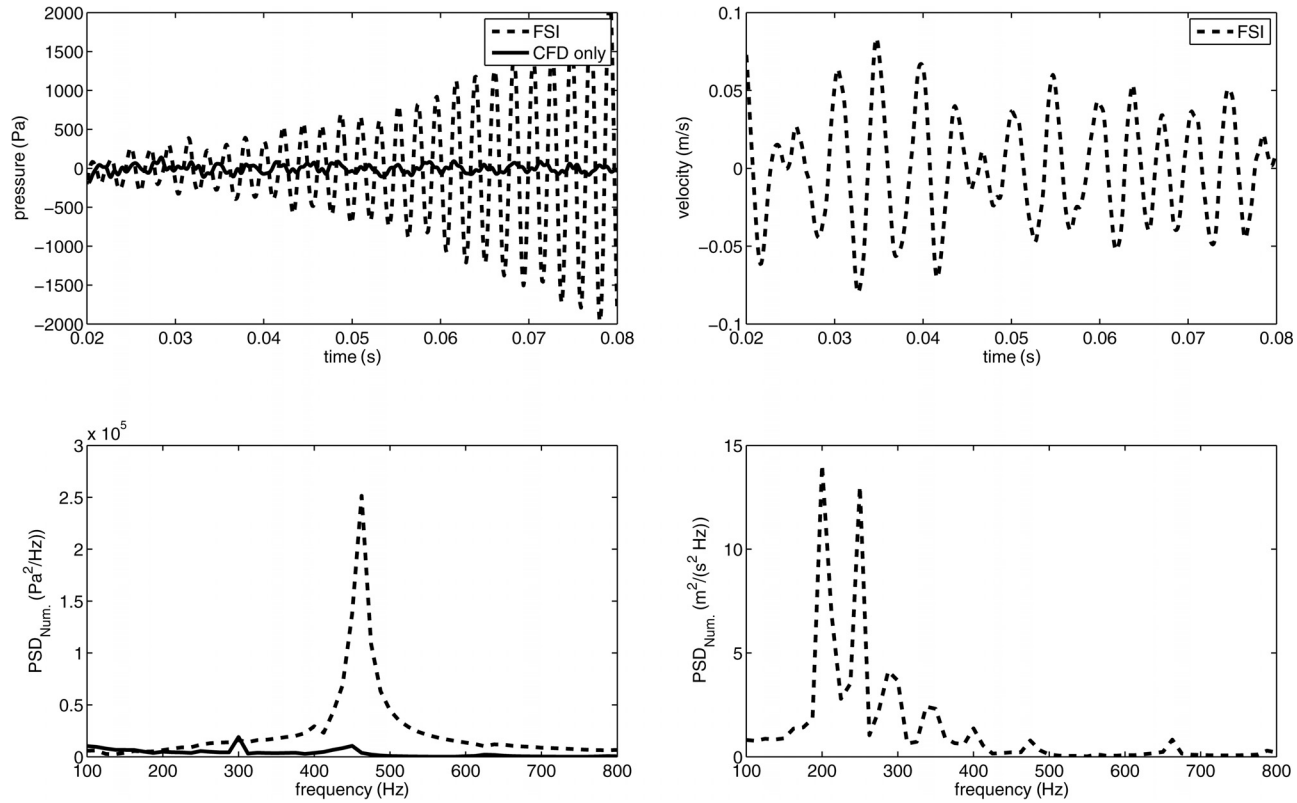

Fig. 10 Numerical results of the pressure and velocity signal in time and frequency domain for the uniform liner configuration

instabilities, which arise within 0.1 s to almost saturation level. Considering this operating point in the conventional CFD analysis without taking into account vibrating walls would lead to major underestimation of the instabilities (see Fig. 10).

7 Conclusions

Numerical investigation of the fluid-structure interaction between the combusting flow inside the combustion chamber, acoustics induced by the flame fluctuations, and liner walls vibrations has been performed. Three different geometries were analyzed numerically in order to predict pressure fluctuations and liner vibrations. A partitioning, two-way interaction scheme was used. The results of the CFD analysis were successfully linked with the FEM code and vice versa. The outcome of the computations was validated with experimental data (for two cases).

Numerical results have revealed an underprediction of the amplitude of the pressure fluctuations compared to the experiment. The obtained inaccuracy was caused mainly due to the numerical damping of the acoustic wave in the CFD code, simplifications done to the fluid and structural domains, and limited computational time. For the latter, it was expected that the combustion instabilities could not grow up to the level observed during the experimental research. In the aftermath of the above, also smaller mechanical loads were transferred to the FEM code and reduced liner velocities were predicted.

Even though the computed pressure and velocity amplitudes were generally underestimated, the hazardous frequencies were marked correctly (with error of 2%–6%). This suggests a linear behavior of the acoustic system. Next to the forcing peak at 300 Hz, all the thermoacoustic instabilities located in the frequency range of 430–460 Hz were visible on the pressure spectrum. Also, the secondary instabilities at around 610–640 Hz were present in the numerical results. Similar behavior was observed for the velocity signal. For the flexible liner configuration, the main frequency of vibration was recognized by the numerical codes around 220–250 Hz, whereas the experimental results have pointed out a competition between vibrational frequencies of 236 Hz and 418 Hz. Apparently, the system can switch between these modes.

The uniform liner configuration simulation shows the instabilities at a similar frequency as the other two configurations, i.e., in the vicinity of the second acoustic mode. However, the amplitude of the acoustic fluctuations inside the combustion chamber rapidly grows to saturation level. This behavior indicates that, for the same operating conditions, the instabilities can be triggered and enhanced/damped by the liner configuration. In this case, the acoustic energy added by the vibrating wall, in the vicinity of the flame, to the burner velocity fluctuations, leading to increased fluctuations of the heat released, has major impact on the thermoacoustic instabilities. It can be concluded that, for problems where interaction between the flame and walls phenomena is strong, the two-way fluid-structure interaction is important and should be taken into account.

Acknowledgment

This work was performed within the EU-sponsored project FLUISTCOM, contract number MRTN-CT-2003-504183.

References

[1] Tinga, T., van Kampen, J. F., De Jager, B., and Kok, J. B. W., 2007, "Gas Turbine Combustor Liner Life Assessment Using a Combined Fluid/Structural Approach," ASME J. Eng. Gas Turbines Power, **129**(1), pp. 69–79.
[2] Ducruix, S., Schuller, T., Durox, D., and Candel, S., 2003, "Combustion Dynamics and Instabilities: Elementary Coupling and Driving Mechanisms," J. Propuls. Power, **19**(5), pp. 722–734.
[3] Lieuwen, T., Torres, H., Johnson, C., and Zinn, B. T., 2001, "A Mechanism of Combustion Instability in Lean Premixed Gas Turbine Combustors," ASME J. Eng. Gas Turbines Power, **123**(1), pp. 182–189.
[4] Hubbard, S., and Dowling, A. P., 2001, "Acoustic Resonances of an Industrial Gas Turbine Combustion System," ASME J. Eng. Gas Turbines Power, **123**(4), pp. 766–773.

[5] Rayleigh, J. W. S., 1878, "The Explanation of Certain Acoustic Phenomena," Nature, **18**, pp. 319–321.
[6] Chu, B. T., 1964, "On the Energy Transfer to Small Disturbances in Fluid Flow (Part 1)," Acta Mech., **1**(3), pp. 215–234.
[7] Dowling, A. P., 1995, "The Calculation of Thermoacoustic Oscillations," J. Sound Vib., **180**(4), pp. 557–581.
[8] Lieuwen, T., 2003, "Combustion Driven Oscillations in Gas Turbines," Turbomach. Int., **44**, pp. 16–18.
[9] Cho, J., and Lieuwen, T., 2005, "Laminar Premixed Flame Response to Equivalence Ratio Oscillations," Combust. Flame, **140**(1–2), pp. 116–129.
[10] Hemchandra, S., Peters, N., and Lieuwen, T., 2011, "Heat Release Response of Acoustically Forced Turbulent Premixed Flames—Role of Kinematic Restoration," Proc. Combust. Inst., **33**(1), pp. 1609–1617.
[11] Kim, K. T., and Hochgreb, S., 2012, "Effects of Nonuniform Reactant Stoichiometry of Thermoacoustic Instability in a Lean-Premixed Gas Turbine Combustor," Combust. Sci. Technol., **184**(5), pp. 1–21.
[12] Komarek, T., and Polifke, W., 2010, "Impact of Swirl Fluctuations on the Flame Response of a Perfectly Premixed Swirl Burner," ASME J. Eng. Gas Turbines Power, **132**(6), p. 061503.
[13] Breard, C., Sayma, A. I., Vahdati, M., and Imregun, M., 2002, "Aeroelasticity Analysis of an Industrial Gas Turbine Combustor Using a Simplified Combustion Model," J. Fluids Struct., **16**(8), pp. 1111–1126.
[14] Khatir, Z., Pozarlik, A. K., Cooper, R. K., Watterson, J. W., and Kok, J. B. W., 2008, "Numerical Study of Coupled Fluid-Structure Interaction for Combustion System," Int. J. Numer. Methods Fluids, **56**(8), pp. 1343–1349.
[15] Huls, R. A., Sengissen, A. X., van der Hoogt, P. J. M., Kok, J. B. W., Poinsot, T., and de Boer, A., 2007, "Vibration Prediction in Combustion Chambers by Coupling Finite Elements and Large Eddy Simulations," J. Sound Vib., **304**(1–2), pp. 224–229.
[16] Dhopade, P., Neely, A. J., and Young, J., 2010, "Fluid-Structure Interaction of Gas Turbine Blades," 17th Australasian Fluid Mechanics Conference, Auckland, New Zealand, December 5–9.
[17] Gorla, R. S. R., Pai, S. S., and Rusick, J. J., 2003, "Probabilistic Study of Fluid Structure Interaction," Int. J. Eng. Sci., **41**(3–5), pp. 271–282.
[18] Lieuwen, T. C., 1999, "Investigation of Combustion Instability Mechanism in Premixed Gas Turbines," Ph.D. thesis, Georgia Institute of Technology, Atlanta, GA.
[19] Fannin, C. A., 2000, "Linear Modelling and Analysis of Thermoacoustic Instabilities in a Gas Turbine Combustor," Ph.D. thesis, Virginia Polytechnic Institute and State University, Blacksburg, VA.
[20] Pozarlik, A. K., and Kok, J. B. W., 2012, "Experimental Investigation and Numerical Prediction of Thermo-Acoustic Instabilities and Associated Liner Vibrations Induced by Turbulent Combustion in Gas Turbines," 50th AIAA Aerospace Sciences Meeting, Nashville, TN, January 9–12, AIAA Paper No. 2012-0354.
[21] Spectral Dynamic, 2001, "DSP-SigLab User Guide," Spectral Dynamic, Fremont, CA.
[22] ANSYS, 2007, "ANSYS CFX User's Guide, Release 11.0," ANSYS, Inc., Canonsburg, PA.
[23] ANSYS, 2007, "ANSYS Coupled-Field Analysis Guide, Release 11.0," ANSYS, Inc., Canonsburg, PA.
[24] Lighthill, M. J., 1952, "On Sound Generated Aerodynamically, I. General Theory," Proc. R. Soc. London, A, **211**(1107), pp. 564–587.
[25] Lighthill, M. J., 1954, "On Sound Generated Aerodynamically II. Turbulence as a Source of Sound," Proc. R. Soc. London, A, **222**(1148), pp. 1–31.
[26] Klein, S. A., 2000, "On the Acoustics of Turbulent Non-Premixed Flames," Ph.D. thesis, University of Twente, Enschede, Netherlands.
[27] Lefebvre, A. H., 1983, *Gas Turbine Combustion*, Hemisphere, Bristol, PA.
[28] Poinsot, T., and Veynante, D., 2005, *Theoretical and Numerical Combustion*, 2nd ed., Edwards, Philadelphia, PA.
[29] Menter, F. R., Kuntz, M., and Bender, R., 2003, "A Scale-Adaptive Simulation Model for Turbulent Flow Predictions," 41st Aerospace Sciences Meeting and Exhibit, Reno, NV, January 6–9, AIAA Paper No. 2003-767.
[30] Menter, F. R., and Egorov, Y., 2005, "Scale-Adaptive Simulation für Technische Strömungen (Scale-Adaptive Simulation for Fluid Flow)," Technology Day 2005, ERCOFTAC Pilot Center Germany South, Stuttgart, Germany, September 30.
[31] Pozarlik, A. K., and Kok, J. B. W., 2008, "Numerical Prediction of Interaction Between Combustion, Acoustics and Vibration in Gas Turbines," 155th Meeting of the Acoustical Society of America (Acoustics '08), Paris, June 29–July 4, pp. 2749–2754.
[32] Rotta, J. C., 1972, *Turbulente Strömungen: Eine Einführung in die Theorie und ihre Anwendung (Turbulent Flows: An Introduction to the Theory and Its Application)*, Teubner, Stuttgart, Germany.
[33] Blom, C., 2003, "Discontinuous Galerkin Method on Tetrahedral Elements for Aeroacoustics," Ph.D. thesis, University of Twente, Enschede, Netherlands.
[34] Tam, C. K. W., 1995, "Computational Aeroacoustics: Methods and Applications," AIAA J., **33**(10), pp. 1788–1796.
[35] Felippa, C. A., Park, K. C., and Farhat, C., 2001, "Partitioned Analysis of Coupled Mechanical Systems," Comput. Methods Appl. Mech. Eng., **190**(24–25), pp. 3247–3270.
[36] Hermann, M. G., and Steindorf, J., 2003, "Partitioned Strong Coupling Algorithms for Fluid-Structure Interaction," Comput. Struct., **81**(8–11), pp. 805–812.
[37] Farath, C., Lesoinne, M., and Le Tallec, P., 1998, "Load and Motion Transfer Algorithms for Fluid/Structure Interaction Problems With Non-Matching Discrete Interfaces: Momentum and Energy Conservation, Optimal Discretization and Application to Aeroelasticity," Comput. Methods Appl. Mech. Eng., **157**(1–2), pp. 95–114.
[38] De Boer, A., Van Zuijlen, A. H., and Bijl, H., 2007, "Review of Coupling Methods for Non-Matching Meshes," Comput. Methods Appl. Mech. Eng., **196**(8), pp. 1515–1525.
[39] Forsythe, N. A., 2006, "A Partitioned Approach to Fluid-Structure Interaction for Artificial Heart Valves," Ph.D. thesis, Queen's University Belfast, Belfast, UK.
[40] Hubner, B., and Seidel, U., 2007, "Partitioned Solution to Strongly Coupled Hydroelastic Systems Arising in Hydro Turbine Design," 2nd IAHR International Meeting of the Workgroup on Cavitation and Dynamic Problems in Hydraulic Machinery and Systems, Timisoara, Romania, October 24–26, pp. 55–64.
[41] Hameyer, K., Driesen, J., De Gersem, H., and Belmans, R., 1999, "The Classification of Coupled Field Problems," IEEE Trans. Magn., **35**(3), pp. 1618–1621.